This is an open access article published under an ACS AuthorChoice License, which permits copying and redistribution of the article or any adaptations for non-commercial purposes.

ACS OMEGA

http://pubs.acs.org/journal/acsodf

Article

Poly(lauryl methacrylate)-Grafted Amino-Functionalized Zirconium-Terephthalate Metal−Organic Framework: Efficient Adsorbent for Extraction of Polycyclic Aromatic Hydrocarbons from Water Samples

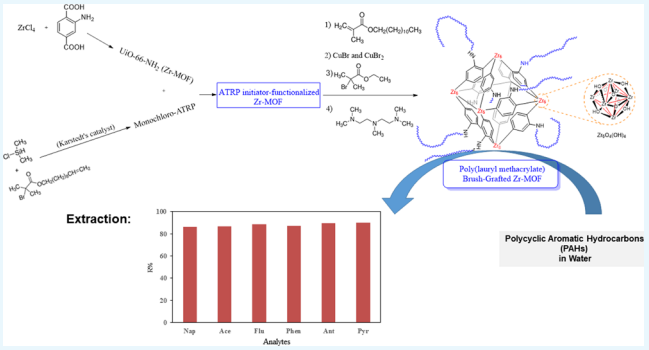
Maryam Tabatabaii, Mostafa Khajeh,* Ali Reza Oveisi, Mustafa Erkartal, and Unal Sen*

Cite This: *ACS Omega* 2020, 5, 12202−12209

Read Online

ACCESS | Metrics & More | Article Recommendations | Supporting Information

ABSTRACT: In this study, a novel porous hybrid material, poly(lauryl methacrylate) polymer-grafted UiO-66-NH_2 (UiO = University of Oslo), was synthesized for efficient extraction of polycyclic aromatic hydrocarbons (PAHs) from aqueous samples. The polymer end-tethered covalently to the MOF's surface was synthesized by surface-initiated atom transfer radical polymerization, revealing a distinct type of morphology. The adsorbent was characterized by scanning electron microscopy, energy-dispersive spectroscopy, transmission electron microscopy, powder X-ray diffraction, N_2 adsorption−desorption analysis, Fourier transform infrared spectroscopy, and thermogravimetric analysis. The analyses were carried out by gas chromatography−mass spectrometry. Parameters including the type and volume of the eluent, the amount of the adsorbent, and adsorption and desorption times were investigated and optimized. Under optimal conditions, the limit of detection, intraday precision, and interday precision were in the range of 3−8 ng L^{-1}, 1.4−3.1, and 4.1−6.5%, respectively. The procedure was used for analysis of PAHs from natural water samples.



1. INTRODUCTION

Metal−organic frameworks (MOFs) self-assembled from the coordination of metal ions or clusters with organic linkers are classes of novel crystalline synthetic porous materials, which exhibit outstanding features, such as permanent porosity, ultrahigh specific surface areas, low densities, and large structural diversity.[1−3] These frameworks can be tailored toward specific applications, such as gas storage,[4,5] chemical separations,[6−8] removal of heavy metals and toxic chemicals,[9−12] and catalysis.[13−16] However, the fragile nature and poor processibility of pure MOFs make them difficult for some applications.[17−20] To solve such problems, hybrid MOF materials, combining MOFs with other materials, have been recently reported.[21−28] When an MOF combines with a polymer, the characteristics of the new obtained material is improved as compared to the pristine phase, benefiting from synergistic interplay between rigid MOFs and flexible polymers.[22,24,26,27,29,30] However, these hybrid materials generally suffered from drawbacks, such as the pore blocking of MOFs by polymers and poor compatibility between the components. Recent research has shown that "grafting from" method or polymer-grafted MOFs are an efficient strategy in the functionalization of the MOF surface with polymer chains.[27,31−33] Despite these successful achievements, a straightforward and efficient modification method, producing porous MOF/polymer hybrids with tailored surface functionalities, is challenging.

Polycyclic aromatic hydrocarbons (PAHs) are widespread environmental organic pollutants that cause carcinogenic, toxic, mutagenic, and potential immune-suppressant effects.[34,35] Therefore, the introduction of a rapid and effective method for extraction and determination of PAHs in environmental samples (spatially in aqueous media) is still demanded.[36−40] Accordingly, considerable research has been recently conducted to illustrate new types of sorbents such as porphyrin-based magnetic nanocomposites,[37] Fe@MIL-101(Cr) MOF,[38] indium(III) sulfide@MOF,[39] and magnetic MIL-100 MOF[40] for preconcentration and extraction of PAHs. Although these procedures have promoted their application for removal of PAHs, the detection limit of these methods is relatively high.

MOF−polymer hybrids, in which polymers are forming a part of a highly porous lattice, are currently being investigated as selective and excellent sorbents.[21−23,41−43] Combining

Received: February 15, 2020
Accepted: April 23, 2020
Published: May 20, 2020



Downloaded via 78.187.196.149 on February 7, 2022 at 09:47:49 (UTC).
See https://pubs.acs.org/sharingguidelines for options on how to legitimately share published articles.

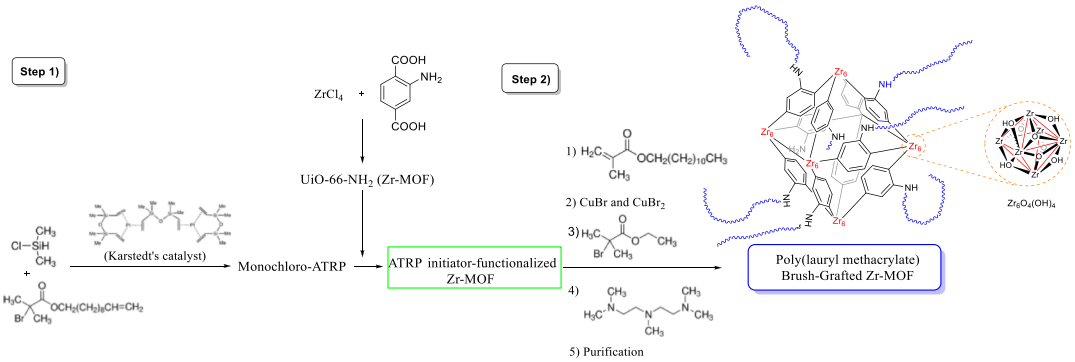


Figure 1. Synthetic steps for the preparation of the polymer-grafted MOF.

MOFs and polymers can enhance stability, selectivity, and solubility of the hybrid material in a solvent beyond those obtained by the individual components[23,43] which are desirable for separation processes.[44,45] Surface-initiated atom transfer radical polymerization (SI-ATRP) is a highly developed technique for high degree of grafting "soft" polymers on MOFs.[31,46−50] This strategy contains polymerization from active sites on the MOF, allowing the controlled growth of the polymer from initiator points.[44,48] Moreover, the SI-ATRP method has been proven to maintain the framework structure of the pristine MOF during the process.

Hence, in the present study, a new polymer-grafted UiO-66-NH_2 MOF was synthesized, containing an MOF as the core and a layer of poly(lauryl methacrylate) (PLMA) tethered covalently on the MOF's surface. UiO-66-NH_2, containing 2-aminoterephthalate (H_2NBDC) units, was selected as a support because of its robustness and structural stability.[51] An in situ-produced monochlorosilane-terminated ATRP initiator[44,52] was installed onto the surface of the MOF. Then, the resultant MOF was modified postsynthetically by polymer chains using copper catalysis, pentamethyldiethylenetriamine (PMDETA), ethyl 2-bromoisobutyrate, and LMA to give the final solid hybrid, polymer@UiO-66-NH_2. Finally, the new hybrid sorbent was tested for the solid-phase extraction[53−58] of PAHs.

2. RESULTS AND DISCUSSION

2.1. Characterization of the Composite. Figure 1 shows schematically the synthesis of poly(lauryl methacrylate)-grafted UiO-66-NH_2. The porous UiO-66-NH_2, containing the 2-aminoterephthalate linker, fabricated using the solvothermal method was first postsynthetically functionalized by the reaction of the amine groups of the MOF with the in situ-formed monochlorosilane-terminated ATRP monomer. 11-(Chlorodimethylsilyl)undecenyl bromoisobutyrate was obtained by the reaction of 10-undecenyl 2-bromoisobutyrate and chlorodimethylsilane in the presence of Karstedt's catalyst[44] (see Experimental Section), giving the ATRP initiator-functionalized Zr-MOF (Figure 1, step-1). Then, the resultant solid served as a core for the growth of the polymer layer using copper, PMDETA, ethyl 2-bromoisobutyrate, and lauryl methacrylate, attaching covalently the poly(lauryl methacrylate) chains to the MOF's amine groups by one end, denoted here as polymer-grafted MOF (polymer@MOF, Figure 1, step-2).

The copper and PMDETA were used as a catalytic system mediating ATRP.[52] Ethyl 2-bromoisobutyrate was served as a free inhibitor to control the polymerization process.[44] The polymer chains on UiO-66-NH_2 nanoparticles were characterized by FT-IR spectroscopy (Figures S1−S3). As seen, the peaks appeared at ∼2928 cm^{-1} are related to the C−H stretching vibration of the aliphatic chains. The new peak appeared at 1101 cm^{-1} and the intense peak at 1665 cm^{-1}, respectively, related to the stretching vibration of C−O and C═O groups of the polymer were associated with the disappearance of −NH_2 stretching modes of UiO-66-NH_2 at 3365 and 3350 cm^{-1}. This indicates the presence of the initiator and the polymer covalently bonded on the MOF (Figure S3). The successful formation of postsynthetic polymerization and its effect on the porosity of the composite were further assessed by N_2 sorption measurements at 77 K (Figure 2).

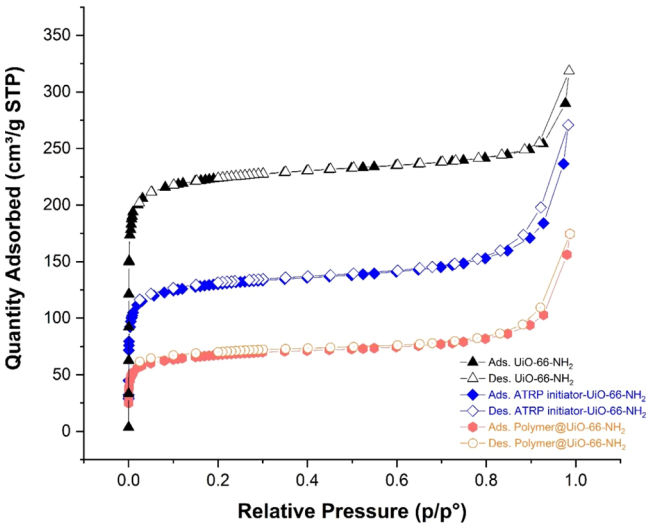


Figure 2. Nitrogen adsorption−desorption isotherms of UiO-66-NH_2 (top), ATRP initiator Zr-MOF (middle), and polymer-grafted Zr-MOF (bottom).

Isothermal nitrogen adsorption−desorption measurements show that the three materials have type I isotherms with surface areas of 900, 550, and 200 m^2 g^{-1}, corresponded to UiO-66-NH_2, ATRP initiator-functionalized UiO-66-NH_2, and polymer@UiO-66-NH_2, respectively. A decrease in the BET surface areas from the parent MOF to the ATRP initiator-functionalized UiO-66-NH_2 and to the polymer@MOF is attributed to the occupied space by immobilizing the ATRP initiator and the growing polymer chains, respectively. This emphasizes the successful postsynthetic modification (PSM) processes on the UiO-66-NH_2 MOF. Furthermore, the main

https://dx.doi.org/10.1021/acsomega.0c00687
ACS Omega 2020, 5, 12202−12209

decrease in the BET surface area may be due to the additional mass of the nonporous polymer, which does not contribute significantly to the surface area. Using the N_2 isotherm, the pore diameters of the porous material (polymer@MOF) were found in the range of about 9−12.6 Å, as shown in Figure S4.

Powder X-ray diffraction (PXRD) patterns of simulated UiO-66(Zr)-NH_2 (CCDC no. 889529),[22,59] UiO-66(Zr)-NH_2, ATRP initiator-functionalized UiO-66(Zr)-NH_2, and polymer@UiO-66(Zr)-NH_2 demonstrate that the structures are isostructural and the UiO-66-NH_2 framework preserves its structure after PSMs (Figure S5). The observed decrease in the intensity of some peaks of the polymer@UiO-66-NH_2 pattern is likely related to the existence of an amorphous polymer in the composite. The main reflection peaks at 2θ = 7.4, 8.6, 6.6, 12.1, 22.3, and 25.7° corresponded to the (1 1 1), (2 0 0), (2 2 0), (5 1 1), and (6 0 0) Miller indices as observed for the simulated XRD pattern of UiO-66-NH_2.[14,22,59]

Thermogravimetric analysis (TGA) of the solid displays two distinct changes at around 290 and 440 °C related to decomposition of the grafted polymer, and subsequently, decomposition of UiO-66-NH_2 (Figure S6). According to TGA measurement, the amount of the polymer in the composite was calculated to be about 23 wt %. Energy-dispersive X-ray spectroscopy (EDS) coupled with scanning electron microscopy (SEM) was used to confirm the PSMs. SEM images of UiO-66-NH_2 show cubic crystalline structures ranging from ∼60 to ∼220 nm in diameter (Figure 3).

Interestingly, the SEM images of the polymer-grafted MOF were different from those of the pristine MOF and exhibited morphology structural forms in which the MOF nanoparticles are well-embedded in the polymer (Figure 3a−d). The observed morphology could be attributed to polymer deformation and the strong affinity between the MOF and polymer.[60]

From EDS analyses, a marked increase in carbon content with a reduction in Zr content was observed for the polymer@MOF relative to the parent MOF (Figure S7, Tables S1 and S2). These observations approve the formation of the polymer on the surface of the MOF as the polymer-grafted MOF NPs. Furthermore, the morphology of the polymer@MOF composite was assessed by transmission electron microscopy (TEM), as displayed in Figure S8. The high-resolution images indicate that the UiO-66-NH_2 nanoparticles are dispersed individually and uniformly in the thin polymer matrix. The data confirm the success in the preparation of the composite. It should be noted that increase in the molar ratio monomers results in the pore blocking of the MOF and the appearance of the new peaks in PXRD patterns (Figures S9 and S10).

2.2. Optimization of Extraction Conditions. To optimize the extraction conditions, several parameters including the amount of the adsorbent, extraction time, the type and volume of the eluent (desorption), and elution time have been considered. Effects of different amounts of the polymer@MOF in the range of 1.0−10.0 mg were studied on the extraction recovery (R %). As shown in Figure 4, R % increases with the increase in the amount of the adsorbent from 1.0 to 3.0 mg. When the mass of the adsorbent is higher than 3.0 mg, the recovery remains almost constant. This could be contributed to the increase in the contact surface area and active sites for PAH adsorption caused by the enhancement of the amount of the adsorbent. Therefore, 3.0 mg of the adsorbent was used as the optimum amount of the adsorbent in the next experiments.

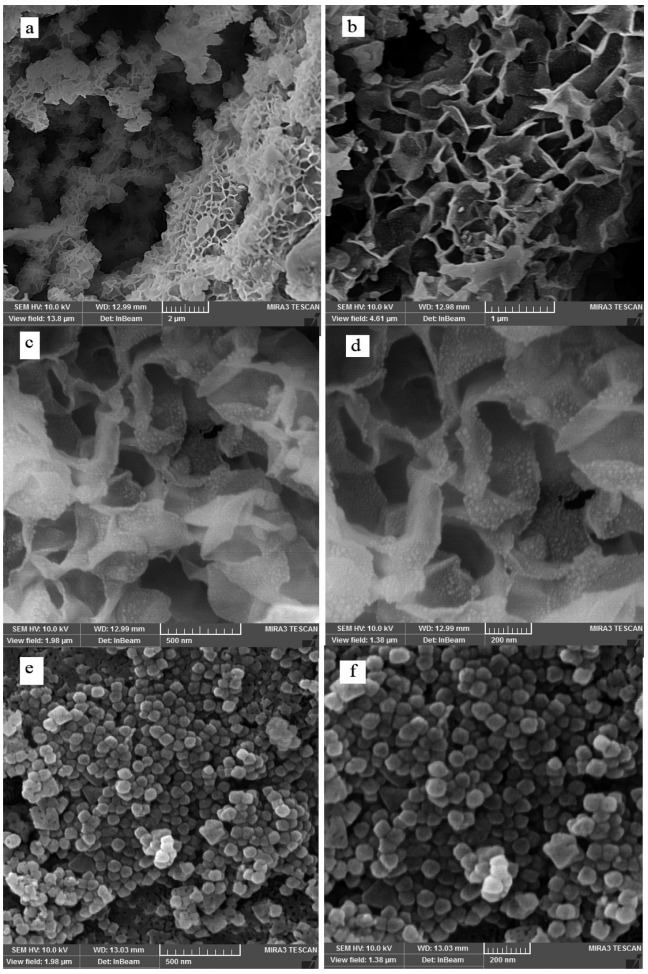


Figure 3. SEM images of the polymer@Zr-MOF (a−d) and Zr-MOF (e,f) with different magnifications.

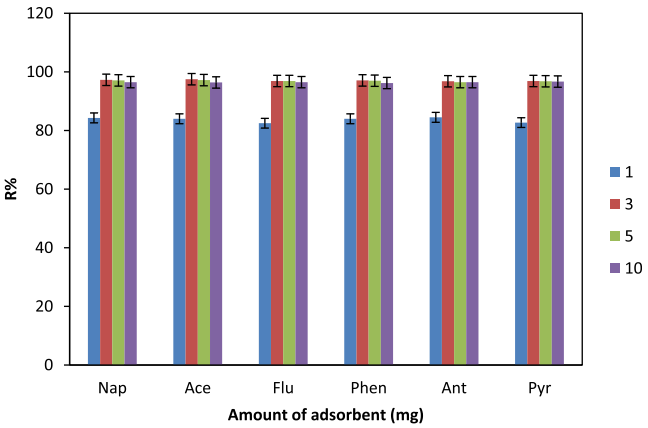


Figure 4. Effect of the amount of the sorbent on the extraction efficiency of PAHs (extraction time = 10 min; eluent = ethanol; desorption time = 2 min; and eluent volume = 0.4 mL).

The extraction time is another factor that affects the extraction recovery. In this study, the effect of extraction time on R % was considered in the range of 2.0−10.0 min. As shown in Figure 5, the extraction recovery of PAHs increases up to 5.0 min and then remained constant because of achieving the extraction equilibrium. Therefore, 5.0 min was chosen as extraction time in the subsequent experiments.

https://dx.doi.org/10.1021/acsomega.0c00687
ACS Omega 2020, 5, 12202−12209

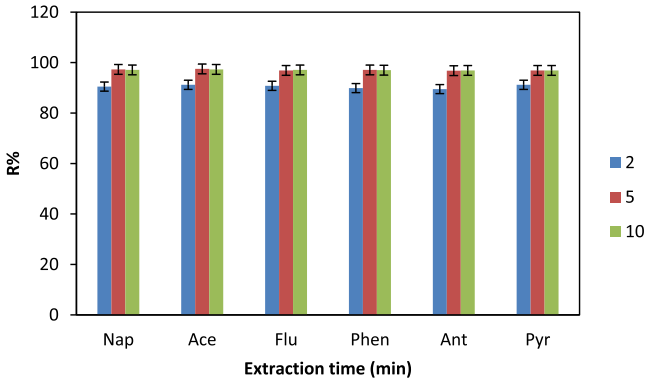


Figure 5. Effect of extraction time on the extraction efficiency of PAHs (amount of adsorbent = 3 mg; eluent = ethanol; desorption time = 2 min; and eluent volume = 0.4 mL).

The desorption process is a key important step in achieving a high extraction recovery and reusability of the adsorbent. The use of the adsorbent is limited when the desorption is incomplete. After extraction of target compounds from aqueous solution, their desorption from the adsorbent is needed to be optimized. Therefore, the type of elution (desorption) solvent affecting the extraction recovery was considered (Figure 6). As shown in Figure 6, three solvents including *n*-hexane, acetonitrile, and ethanol were examined. The results show that ethanol has the best efficiency.

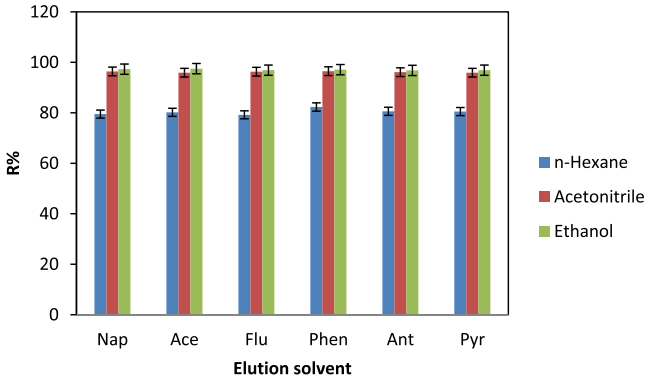


Figure 6. Effect of the desorption solvent on the extraction recovery (amount of adsorbent = 3 mg; extraction time = 5 min; desorption time = 2 min; and eluent volume = 0.4 mL).

According to Figure S11, optimization of the elution solvent volume indicates that *R* % reaches the maximum when the elution volume is 300 μL. Therefore, 300 μL of elution solvent was used for desorption of PAHs in next experiments. Then, the desorption time was examined in the range of 1.0−10.0 min. As shown in Figure S12, the maximum desorption recovery is obtained in 2.0 min, and after this time, the efficiency decreases slightly. This phenomenon could be attributed to the readsorption of the target compounds to the adsorbent.[37,61] Therefore, 2.0 min was used as the desorption time for next experiments.

According to the abovementioned observations, the best *R* % was obtained using 3.0 mg of adsorbent, extraction time of 5.0 min, 300.0 μL of ethanol, and 2.0 min desorption time.

The reusability of the adsorbent is another important parameter. In this study, the reusability of the adsorbent was then investigated. Therefore, the reusability of the adsorbent for extraction of target PAHs was tested, followed by washing with ethanol as the eluent. The experiments showed that the adsorbent could be reused at least ten times by <3.1% loss in *R* %. These results indicate that the composite has the potential to be used as a recyclable sorbent.

2.3. Extraction Recovery Comparison of the Polymer@MOF and MOF. The extraction recovery of the spiked water samples (C = 1.0 μg L^{-1}, n = 3, six PAHs) was carried out with UiO-66-NH_2 MOF and polymer@MOF for comparison, as the results are shown in Figure 7. The polymer@MOF composite shows higher extraction recovery for PAHs compared to the pristine MOF (Figure 7).

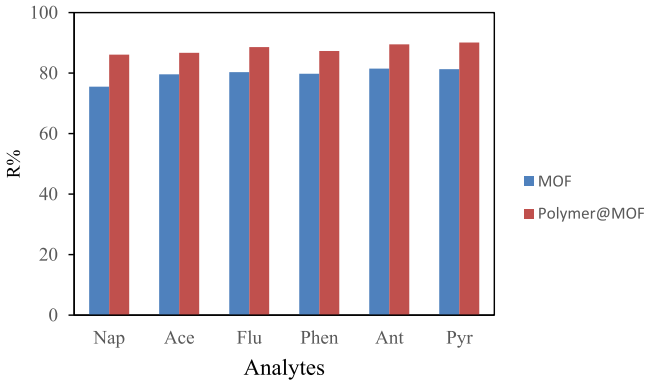


Figure 7. Comparison of the polymer@UiO-66-NH_2 with UiO-66-NH_2 for PAH extraction (amount of adsorbent = 3 mg; extraction time = 5 min; eluent = ethanol; desorption time = 2 min; and eluent volume = 0.4 mL).

2.4. Validation of the Procedure. To validate the extraction recovery of the adsorbent, the calibration curves, correlation coefficients, limits of detection (LODs), intraday precisions, and interday precisions were investigated under the optimized conditions for target compounds. The results are displayed in Table 1.

Table 1. Figures of Merit of the Proposed Method

compound	*R*	LOD[a]	linear range (μg L^{-1})	intraday precision (%)	interday precision (%)
Nap	0.9997	3	0.01−15	2.4	4.1
Ace	0.9991	4	0.02−13	2.7	5.5
Flu	0.9998	5	0.03−13	2.2	4.8
Phen	0.9991	8	0.035−12	3.1	5.2
Ant	0.9993	7	0.025−12	1.4	6.5
Pyr	0.9992	8	0.03−12	2.5	5.3

[a]LOD, limit of detection in ng L^{-1}.

Good linear correlations were obtained with R^2 > 0.999 for all target compounds in a range of about 10−15,000 ng L^{-1}. Also, the precision of the procedure was evaluated by intraday repeatability and interday reproducibility. The relative standard deviations (RSD %, n = 5) of repeatability and reproducibility were less than 3.1 and 6.5%, respectively. The detection limits (S/N = 3) of target compounds ranged from 3 to 8 ng L^{-1}.

Table 2 shows the comparisons among the results obtained by polymer@UiO-66-NH_2 and previously reported procedures. The results present that the LOD of this procedure has better values than those in other methods. Also, the composite

https://dx.doi.org/10.1021/acsomega.0c00687
ACS Omega 2020, 5, 12202−12209

Table 2. Comparison of the MOF Procedure with Other Related Methods for Determination of PAHs

extraction method	detection	LOD (ng L^{-1})	extraction time (min)	organic solvent consumption (mL)	RSD %	ref.
porphyrin-based magnetic nanocomposite	GC−MS	2.0−10.0	10.0	2.0	3.1−7.8	37
Fe@MIL-101(Cr)	GC−MS	80−200	40.0	0.4	4.1−6.3	38
indium(III) sulfide@MOF	GC−MS	2.9−83	35.0	2.0	2.6−9.2	39
magnetic MIL-100 MOF	GC−FID	4.6−8.9	20.0	0.5	1.7−9.8	40
polymer@Zr-MOF	GC−MS	3.0−8.0	5.0	0.3	1.4−3.1	this method

adsorbent indicates good sensitivity with a much lower consumption of the organic solvent.

2.5. Analysis of Real Samples. To analyze the applicability of the suggested sorbent in the solid-phase extraction procedure, target compounds in drinking and ground water samples were analyzed under optimal conditions and the results are represented in Table 3.

Table 3. Determination of the PAHs in Different Water Samples

		spiked (0.5 μg L^{-1})		spiked (1.0 μg L^{-1})	
water samples	analytes	*R* %	RSD %	*R* %	RSD %
drinking water	Nap	98.2	3.5	96.5	2.9
	Ace	96.9	3.9	97.9	2.8
	Flu	97.1	3.1	94.6	2.4
	Phen	94.6	1.9	97.3	2.8
	Ant	95.2	2.8	95.8	1.5
	Pyr	97.5	3.2	96.1	3.1
ground water	Nap	97.1	3.1	95.5	2.9
	Ace	97.9	2.5	96.9	3.0
	Flu	98.9	1.4	98.4	2.5
	Phen	98.2	3.1	95.1	3.7
	Ant	96.4	2.9	97.8	3.4
	Pyr	97.3	2.6	95.9	2.9

The results indicate that there was no analyte in the water samples. Then, the aqueous sample solutions were spiked with 0.5 and 1.0 μg L^{-1}. The extraction recovery and relative standard deviations were calculated (Table 3). Figure 8 indicates GC/MS chromatograms of the target compounds (spiked at a concentration of 1.0 μg L^{-1}) performed under the optimized conditions.

2.6. Adsorption Mechanism. In this adsorbent, the porosity of the MOF and the active sites of flexible polymer chains were combined to give a new multifunctional material containing good permeability with the micropores ranging from 0.9 to 1.3 nm in diameter (Figure S4). The maximum calculated diameter of the target compounds is about 1.2 nm, and hence, it is reasonable that the target compounds can move into the pores and the porosity can act as microenvironments to improve diffusion coefficients. In addition, the hydrophobic and flexible grafted polymer can bridge the gap between MOF particles and assist the transport of the PAH solution *via* the MOF pores, thus resulting in improvement of the adsorption of target molecules.[22,27,62,63] These are the main reasons for the high observed performance.

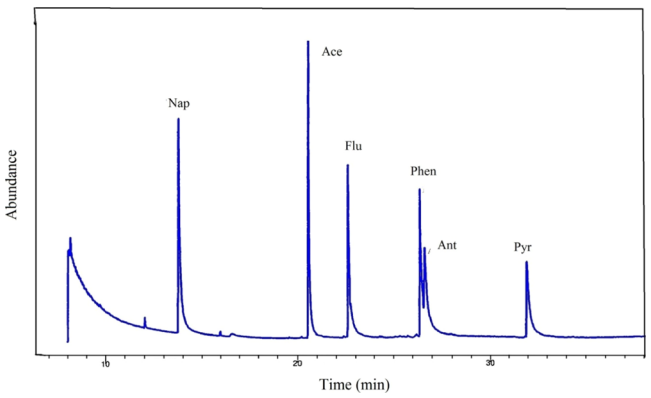


Figure 8. Chromatograms of extract PAHs from water samples (amount of adsorbent = 3 mg; extraction time = 5 min; desorption time = 2 min; and eluent volume = 0.4 mL).

3. CONCLUSIONS

The hybridization of the polymer and UiO-66-NH_2 to produce a novel material (polymer-grafted Zr-MOF) by modifying the surface of the MOF is reported. The porous material was successfully used for removal of PAHs at trace levels in water media. Consequently, the effects of various parameters on extraction efficiency of PAHs were investigated and optimized. The analysis was carried out by gas chromatography/mass spectrometry (GC−MS). The optimal extraction procedure was performed using only 3 mg of the adsorbent for 5 min. Furthermore, the solid-phase extraction method showed low detection limits (3−8.0 ng L^{-1}) and good sensitivity with low consumption of the organic solvent (0.3 mL). The superior performance of the hybrid sorbent as compared to the parent MOF and other materials is possible because of the porosity and the high surface area of the adsorbent and the presence of hydrophobic polymer chains. A fast, reliable, and applicable technique can inspire new methodologies for preparation and application of such materials for a cleaner environment.

4. EXPERIMENTAL SECTION

4.1. Materials. $ZrCl_4$, DMF, acetic acid, 2-aminoterephthalic acid, toluene, chlorodimethylsilane, 10-undecenyl 2-bromoisobutyrate (95%), Karstedt's catalyst in xylene (99%), anisole, ethyl 2-bromoisobutyrate, lauryl methacrylate (LMA, 98%), CuI, CuBr, and *N*,*N*,*N*′,*N*′,*N*″-PMDETA (99%) were purchased from Sigma-Aldrich, Germany. Naphthalene (Nap), fluorine (Flu), acenaphthylene (Ace), anthracene (Ant), phenanthrene (Phe), and pyrene (Pyr) were purchased from Merck (Darmstadt, Germany). CuBr (98%) was agitated in glacial acetic acid for 12 h before being filtered and washed with ethanol, followed by drying under vacuum. The purified CuBr powder was stored in a desiccator. LMA was dissolved in tetrahydrofuran (THF); then, it was passed through a silica gel column to eliminate the inhibitor, and then, THF was removed under high vacuum.

4.2. Extraction Procedure. The extraction of six PAHs from water samples was investigated by the prepared polymer@MOF adsorbent. First, 3.0 mg of the adsorbent was dispersed into 25 mL of aqueous solution containing 10.0

https://dx.doi.org/10.1021/acsomega.0c00687
ACS Omega 2020, 5, 12202−12209

$\mu g\ L^{-1}$ of each analyte. Later, the vial was closed and the mixture was shaken in an ultrasonic bath for 5.0 min for solid-phase extraction. After that, for separating the adsorbent from aqueous solution, the mixture was centrifuged at 4500 rpm for 10.0 min. Next, the adsorbent was transferred to the vial and a certain volume of the elution solvent was added to the vial. Then, the vial was immersed in an ultrasonic bath for enough time to desorb PAHs in the elution solvent. After centrifugation at 4500 rpm for 5.0 min, the solvent was separated. Finally, 1.0 μL of elution solvent was injected into the GC/MS system.

4.3. Synthesis of UiO-66-NH_2. In this study, the UiO-66-NH_2 was synthesized according to the literature procedure.[14,64]

4.4. Synthesis of Poly(lauryl methacrylate)-Grafted UiO-66-NH_2 (PLMA@Zr-MOF). Step (1): mixtures A and B were prepared as follows. A: activated UiO-66-NH_2 (0.3 g) was added to anhydrous toluene (50 mL). About 20 mL of the solvent was then distilled off to eliminate any water (azeotropic distillation); B: 10-undecenyl 2-bromoisobutyrate (186 μL, 0.628 mmol), chlorodimethylsilane (104 μL, 0.936 mmol), and Karstedt's catalyst in xylene (5 μL) were mixed and slowly stirred under a nitrogen atmosphere for 24 h. Then, the mixture A was added to B and this new mixture under a N_2 atmosphere was stirred at 90 °C for 72 h. The resultant nanoparticles were then separated by centrifugation before being washed with DMF. The ATRP initiator-functionalized Zr-MOF was then dried under vacuum. Step (2): the precipitate obtained (100 mg) and anisole (15 mL) were added to a two-necked flask. The mixture was sonicated for 10 min. Then, the resultant mixture was placed in an ice bath, followed by the addition of LMA (1.5 mL), copper(I) bromide (0.004 g), copper(II) bromide (0.002 g), ethyl 2-bromoisobutyrate (1 μL), and PMDETA (10 μL) under a nitrogen atmosphere. The resulting mixture was then heated and slowly stirred at 90 °C for 24 h. Then, the obtained solid was dispersed in methanol (10 mL) and isolated by centrifugation (three times). The PLMA chain-grafted MOF was soaked in methanol for 24 h and centrifuged, followed by drying under vacuum at 100 °C.

■ ASSOCIATED CONTENT

Supporting Information

The Supporting Information is available free of charge at https://pubs.acs.org/doi/10.1021/acsomega.0c00687.

FT-IR spectra, DFT pore size distribution, PXRD patterns, TGA profile, EDS analyses, TEM images, N_2 adsorption/desorption isotherms, effect of the volume of the eluent solvent, and effect of desorption time (PDF)

■ AUTHOR INFORMATION

Corresponding Authors

Mostafa Khajeh − *Department of Chemistry, Faculty of Science, University of Zabol, 98615-538 Zabol, Iran;* orcid.org/0000-0002-7097-2898; Phone: 0098-9151423614; Email: m_khajeh@uoz.ac.ir; Fax: +98-543-2226765

Unal Sen − *Department of Materials Science and Engineering, Faculty of Engineering, Eskisehir Technical University, 26555 Eskisehir, Turkey;* orcid.org/0000-0003-3736-5049; Phone: 0090-5436683807; Email: unalsen@eskisehir.edu.tr; Fax: +90 (222) 321 95 01

Authors

Maryam Tabatabaii − *Department of Chemistry, Faculty of Science, University of Zabol, 98615-538 Zabol, Iran*

Ali Reza Oveisi − *Department of Chemistry, Faculty of Science, University of Zabol, 98615-538 Zabol, Iran;* orcid.org/0000-0002-0075-211X

Mustafa Erkartal − *Department of Materials Science and Nanotechnology Engineering, Abdullah Gul University, 38080 Kayseri, Turkey*

Complete contact information is available at: https://pubs.acs.org/10.1021/acsomega.0c00687

Author Contributions

M.T. fabricated the hybrid materials under supervision of A.R.O. M.T. performed the adsorption experiments. A.R.O characterized the hybrid material and wrote the manuscript with support from M.K., who supervised the project. U.S. co-supervised the project with the assistance of M.E.

Notes

The authors declare no competing financial interest.

■ ACKNOWLEDGMENTS

The financial support from the University of Zabol (grant number: UOZ-GR-9517-1) is gratefully acknowledged.

■ REFERENCES

(1) Safaei, M.; Foroughi, M. M.; Ebrahimpoor, N.; Jahani, S.; Omidi, A.; Khatami, M. A Review on Metal-Organic Frameworks: Synthesis and Applications. *TrAC, Trends Anal. Chem.* **2019**, *118*, 401−425.

(2) Yuan, S.; Feng, L.; Wang, K.; Pang, J.; Bosch, M.; Lollar, C.; Sun, Y.; Qin, J.; Yang, X.; Zhang, P.; Wang, Q.; Zou, L.; Zhang, Y.; Zhang, L.; Fang, Y.; Li, J.; Zhou, H.-C. Stable Metal−Organic Frameworks: Design, Synthesis, and Applications. *Adv. Mater.* **2018**, *30*, 1704303.

(3) Maurin, G.; Serre, C.; Cooper, A.; Férey, G. The New Age of MOFs and of Their Porous-Related Solids. *Chem. Soc. Rev.* **2017**, *46*, 3104−3107.

(4) Li, H.; Li, L.; Lin, R.-B.; Zhou, W.; Zhang, Z.; Xiang, S.; Chen, B. Porous Metal-Organic Frameworks for Gas Storage and Separation: Status and Challenges. *Energy Chem.* **2019**, *1*, 100006.

(5) Gándara, F.; Furukawa, H.; Lee, S.; Yaghi, O. M. High Methane Storage Capacity in Aluminum Metal−Organic Frameworks. *J. Am. Chem. Soc.* **2014**, *136*, 5271−5274.

(6) Sadiq, M. M.; Suzuki, K.; Hill, M. R. Towards Energy Efficient Separations with Metal Organic Frameworks. *Chem. Commun.* **2018**, *54*, 2825−2837.

(7) Li, J.-R.; Sculley, J.; Zhou, H.-C. Metal−Organic Frameworks for Separations. *Chem. Rev.* **2012**, *112*, 869−932.

(8) Herm, Z. R.; Bloch, E. D.; Long, J. R. Hydrocarbon Separations in Metal−Organic Frameworks. *Chem. Mater.* **2014**, *26*, 323−338.

(9) Sun, D. T.; Peng, L.; Reeder, W. S.; Moosavi, S. M.; Tiana, D.; Britt, D. K.; Oveisi, E.; Queen, W. L. Rapid, Selective Heavy Metal Removal from Water by a Metal−Organic Framework/Polydopamine Composite. *ACS Cent. Sci.* **2018**, *4*, 349−356.

(10) Feng, M.; Zhang, P.; Zhou, H.-C.; Sharma, V. K. Water-Stable Metal-Organic Frameworks for Aqueous Removal of Heavy Metals and Radionuclides: A Review. *Chemosphere* **2018**, *209*, 783−800.

(11) Bobbitt, N. S.; Mendonca, M. L.; Howarth, A. J.; Islamoglu, T.; Hupp, J. T.; Farha, O. K.; Snurr, R. Q. Metal−Organic Frameworks for the Removal of Toxic Industrial Chemicals and Chemical Warfare Agents. *Chem. Soc. Rev.* **2017**, *46*, 3357−3385.

(12) Rezaei Kahkha, M. R.; Daliran, S.; Oveisi, A. R.; Kaykhaii, M.; Sepehri, Z. The Mesoporous Porphyrinic Zirconium Metal-Organic Framework for Pipette-Tip Solid-Phase Extraction of Mercury from Fish Samples Followed by Cold Vapor Atomic Absorption Spectrometric Determination. *Food Anal. Methods* **2017**, *10*, 2175−2184.

(13) Daliran, S.; Santiago-Portillo, A.; Navalón, S.; Oveisi, A. R.; Álvaro, M.; Ghorbani-Vaghei, R.; Azarifar, D.; García, H. Cu(II)-Schiff Base Covalently Anchored to MIL-125(Ti)-NH_2 as Heterogeneous Catalyst for Oxidation Reactions. *J. Colloid Interface Sci.* **2018**, *532*, 700−710.
(14) Azarifar, D.; Ghorbani-Vaghei, R.; Daliran, S.; Oveisi, A. R. A Multifunctional Zirconium-Based Metal−Organic Framework for the One-Pot Tandem Photooxidative Passerini Three-Component Reaction of Alcohols. *ChemCatChem* **2017**, *9*, 1992−2000.
(15) Dhakshinamoorthy, A.; Li, Z.; Garcia, H. Catalysis and Photocatalysis by Metal Organic Frameworks. *Chem. Soc. Rev.* **2018**, *47*, 8134−8172.
(16) Ghaleno, M. R.; Ghaffari-Moghaddam, M.; Khajeh, M.; Reza Oveisi, A.; Bohlooli, M. Iron Species Supported on a Mesoporous Zirconium Metal-Organic Framework for Visible Light Driven Synthesis of Quinazolin-4(3H)-Ones through One-Pot Three-Step Tandem Reaction. *J. Colloid Interface Sci.* **2019**, *535*, 214−226.
(17) Czaja, A. U.; Trukhan, N.; Müller, U. Industrial Applications of Metal−Organic Frameworks. *Chem. Soc. Rev.* **2009**, *38*, 1284−1293.
(18) Bennett, T. D.; Horike, S. Liquid, Glass and Amorphous Solid States of Coordination Polymers and Metal−Organic Frameworks. *Nat. Rev. Mater.* **2018**, *3*, 431−440.
(19) Lin, C.-L.; Lirio, S.; Chen, Y.-T.; Lin, C.-H.; Huang, H.-Y. A Novel Hybrid Metal−Organic Framework−Polymeric Monolith for Solid-Phase Microextraction. *Chem.—Eur. J.* **2014**, *20*, 3317−3321.
(20) Car, A.; Stropnik, C.; Peinemann, K.-V. Hybrid Membrane Materials with Different Metal−Organic Frameworks (Mofs) for Gas Separation. *Desalination* **2006**, *200*, 424−426.
(21) Zhang, Y.; Feng, X.; Yuan, S.; Zhou, J.; Wang, B. Challenges and Recent Advances in Mof−Polymer Composite Membranes for Gas Separation. *Inorg. Chem. Front.* **2016**, *3*, 896−909.
(22) Fotovat, H.; Khajeh, M.; Oveisi, A. R.; Ghaffari-Moghaddam, M.; Daliran, S. A Hybrid Material Composed of an Amino-Functionalized Zirconium-Based Metal-Organic Framework and a Urea-Based Porous Organic Polymer as an Efficient Sorbent for Extraction of Uranium(VI). *Microchim. Acta* **2018**, *185*, 469.
(23) Kitao, T.; Zhang, Y.; Kitagawa, S.; Wang, B.; Uemura, T. Hybridization of MOFs and Polymers. *Chem. Soc. Rev.* **2017**, *46*, 3108−3133.
(24) Semino, R.; Moreton, J. C.; Ramsahye, N. A.; Cohen, S. M.; Maurin, G. Understanding the Origins of Metal−Organic Framework/Polymer Compatibility. *Chem. Sci.* **2018**, *9*, 315−324.
(25) Qian, Q.; Wu, A. X.; Chi, W. S.; Asinger, P. A.; Lin, S.; Hypsher, A.; Smith, Z. P. Mixed-Matrix Membranes Formed from Imide-Functionalized Uio-66-Nh2 for Improved Interfacial Compatibility. *ACS Appl. Mater. Interfaces* **2019**, *11*, 31257−31269.
(26) Yu, G.; Zou, X.; Sun, L.; Liu, B.; Wang, Z.; Zhang, P.; Zhu, G. Constructing Connected Paths between Uio-66 and Pim-1 to Improve Membrane Co2 Separation with Crystal-Like Gas Selectivity. *Adv. Mater.* **2019**, *31*, 1806853.
(27) Kalaj, M.; Bentz, K. C.; Ayala, S.; Palomba, J. M.; Barcus, K. S.; Katayama, Y.; Cohen, S. M. Mof-Polymer Hybrid Materials: From Simple Composites to Tailored Architectures. *Chem. Rev.* **2020**, DOI: 10.1021/acs.chemrev.9b00575.
(28) Khan, M.; Yilmaz, E.; Sevinc, B.; Sahmetlioglu, E.; Shah, J.; Jan, M. R.; Soylak, M. Preparation and Characterization of Magnetic Allylamine Modified Graphene Oxide-Poly(vinyl acetate-co-divinylbenzene) Nanocomposite for Vortex Assisted Magnetic Solid Phase Extraction of Some Metal Ions. *Talanta* **2016**, *146*, 130−137.
(29) Jin, P.; Tan, W.; Huo, J.; Liu, T.; Liang, Y.; Wang, S.; Bradshaw, D. Hierarchically Porous Mof/Polymer Composites Via Interfacial Nanoassembly and Emulsion Polymerization. *J. Mater. Chem. A* **2018**, *6*, 20473−20479.
(30) Campbell, J.; Davies, R. P.; Braddock, D. C.; Livingston, A. G. Improving the Permeance of Hybrid Polymer/Metal−Organic Framework (MOF) Membranes for Organic Solvent Nanofiltration (OSN) − Development of Mof Thin Films Via Interfacial Synthesis. *J. Mater. Chem. A* **2015**, *3*, 9668−9674.
(31) McDonald, K. A.; Feldblyum, J. I.; Koh, K.; Wong-Foy, A. G.; Matzger, A. J. Polymer@MOF@MOF: "Grafting from" Atom Transfer Radical Polymerization for the Synthesis of Hybrid Porous Solids. *Chem. Commun.* **2015**, *51*, 11994−11996.
(32) Xie, K.; Fu, Q.; He, Y.; Kim, J.; Goh, S. J.; Nam, E.; Qiao, G. G.; Webley, P. A. Synthesis of Well Dispersed Polymer Grafted Metal−Organic Framework Nanoparticles. *Chem. Commun.* **2015**, *51*, 15566−15569.
(33) Mohmeyer, A.; Schaate, A.; Hoppe, B.; Schulze, H. A.; Heinemeyer, T.; Behrens, P. Direct Grafting-from of Pedot from a Photoreactive Zr-Based MOF−a Novel Route to Electrically Conductive Composite Materials. *Chem. Commun.* **2019**, *55*, 3367−3370.
(34) Kim, K.-H.; Jahan, S. A.; Kabir, E.; Brown, R. J. C. A Review of Airborne Polycyclic Aromatic Hydrocarbons (PAHs) and Their Human Health Effects. *Environ. Int.* **2013**, *60*, 71−80.
(35) Santos, P. M.; del Nogal Sánchez, M.; Pavón, J. L. P.; Cordero, B. M. Determination of Polycyclic Aromatic Hydrocarbons in Human Biological Samples: A Critical Review. *TrAC, Trends Anal. Chem.* **2019**, *113*, 194−209.
(36) Ncube, S.; Madikizela, L.; Cukrowska, E.; Chimuka, L. Recent Advances in the Adsorbents for Isolation of Polycyclic Aromatic Hydrocarbons (PAHs) from Environmental Sample Solutions. *TrAC, Trends Anal. Chem.* **2018**, *99*, 101−116.
(37) Yu, J.; Zhu, S.; Pang, L.; Chen, P.; Zhu, G.-T. Porphyrin-Based Magnetic Nanocomposites for Efficient Extraction of Polycyclic Aromatic Hydrocarbons from Water Samples. *J. Chromatogr. A* **2018**, *1540*, 1−10.
(38) Zhou, Q.; Lei, M.; Wu, Y.; Yuan, Y. Magnetic Solid Phase Extraction of Typical Polycyclic Aromatic Hydrocarbons from Environmental Water Samples with Metal Organic Framework MIL-101(Cr) Modified Zero Valent Iron Nano-Particles. *J. Chromatogr. A* **2017**, *1487*, 22−29.
(39) Jia, Y.; Zhao, Y.; Zhao, M.; Wang, Z.; Chen, X.; Wang, M. Core−Shell Indium (III) Sulfide@Metal-Organic Framework Nanocomposite as an Adsorbent for the Dispersive Solid-Phase Extraction of Nitro-Polycyclic Aromatic Hydrocarbons. *J. Chromatogr. A* **2018**, *1551*, 21−28.
(40) Huo, S.-H.; An, H.-Y.; Yu, J.; Mao, X.-F.; Zhang, Z.; Bai, L.; Huang, Y.-F.; Zhou, P.-X. Pyrolytic in Situ Magnetization of Metal-Organic Framework MIL-100 for Magnetic Solid-Phase Extraction. *J. Chromatogr. A* **2017**, *1517*, 18−25.
(41) Zhang, Z.; Nguyen, H. T. H.; Miller, S. A.; Ploskonka, A. M.; DeCoste, J. B.; Cohen, S. M. Polymer−Metal−Organic Frameworks (PolyMOFs) as Water Tolerant Materials for Selective Carbon Dioxide Separations. *J. Am. Chem. Soc.* **2016**, *138*, 920−925.
(42) Wang, Z.; Ren, H.; Zhang, S.; Zhang, F.; Jin, J. Polymers of Intrinsic Microporosity/Metal−Organic Framework Hybrid Membranes with Improved Interfacial Interaction for High-Performance CO_2 Separation. *J. Mater. Chem. A* **2017**, *5*, 10968−10977.
(43) Gamage, N.-D. H.; McDonald, K. A.; Matzger, A. J. MOF-5-Polystyrene: Direct Production from Monomer, Improved Hydrolytic Stability, and Unique Guest Adsorption. *Angew. Chem., Int. Ed.* **2016**, *55*, 12099−12103.
(44) Wright, R. A. E.; Wang, K.; Qu, J.; Zhao, B. Oil-Soluble Polymer Brush Grafted Nanoparticles as Effective Lubricant Additives for Friction and Wear Reduction. *Angew. Chem., Int. Ed.* **2016**, *55*, 8656−8660.
(45) Zhao, B.; Zhu, L. Mixed Polymer Brush-Grafted Particles: A New Class of Environmentally Responsive Nanostructured Materials. *Macromolecules* **2009**, *42*, 9369−9383.
(46) He, S.; Wang, H.; Zhang, C.; Zhang, S.; Yu, Y.; Lee, Y.; Li, T. A Generalizable Method for the Construction of MOF@Polymer Functional Composites through Surface-Initiated Atom Transfer Radical Polymerization. *Chem. Sci.* **2019**, *10*, 1816−1822.
(47) Xie, K.; Fu, Q.; Webley, P. A.; Qiao, G. G. MOF Scaffold for a High-Performance Mixed-Matrix Membrane. *Angew. Chem., Int. Ed.* **2018**, *57*, 8597−8602.

(48) Schmidt, B. V. K. J. Metal-Organic Frameworks in Polymer Science: Polymerization Catalysis, Polymerization Environment, and Hybrid Materials. *Macromol. Rapid Commun.* **2020**, *41*, 1900333.
(49) Xie, K.; Fu, Q.; Xu, C.; Lu, H.; Zhao, Q.; Curtain, R.; Gu, D.; Webley, P. A.; Qiao, G. G. Continuous Assembly of a Polymer on a Metal−Organic Framework (CAP on MOF): A 30 Nm Thick Polymeric Gas Separation Membrane. *Energy Environ. Sci.* **2018**, *11*, 544−550.
(50) Liu, H.; Zhu, H.; Zhu, S. Reversibly Dispersible/Collectable Metal-Organic Frameworks Prepared by Grafting Thermally Responsive and Switchable Polymers. *Macromol. Mater. Eng.* **2015**, *300*, 191−197.
(51) Bai, Y.; Dou, Y.; Xie, L.-H.; Rutledge, W.; Li, J.-R.; Zhou, H.-C. Zr-Based Metal−Organic Frameworks: Design, Synthesis, Structure, and Applications. *Chem. Soc. Rev.* **2016**, *45*, 2327−2367.
(52) Liénafa, L.; Monge, S.; Robin, J.-J. A Versatile Synthesis of Poly(Lauryl Acrylate) Using N-(N-Octyl)-2-Pyridylmethanimine in Copper Mediated Living Radical Polymerization. *Eur. Polym. J.* **2009**, *45*, 1845−1850.
(53) Ramos, L. Basics and Advances in Sampling and Sample Preparation. In *Chemical Analysis of Food: Techniques and Applications*; Picó, Y., Ed.; Academic Press: Boston, 2012; Chapter 1, pp 3−24.
(54) Khajeh, M.; Laurent, S.; Dastafkan, K. Nanoadsorbents: Classification, Preparation, and Applications (with Emphasis on Aqueous Media). *Chem. Rev.* **2013**, *113*, 7728−7768.
(55) Menghwar, P.; Yilmaz, E.; Soylak, M. A Hybrid Material Composed of Multiwalled Carbon Nanotubes and Mose2 Nanorods as a Sorbent for Ultrasound-Assisted Solid-Phase Extraction of Lead(II) and Copper(II). *Microchim. Acta* **2019**, *186*, 666.
(56) Khajeh, M.; Golzary, A. R. Synthesis of Zinc Oxide Nanoparticles−Chitosan for Extraction of Methyl Orange from Water Samples: Cuckoo Optimization Algorithm−Artificial Neural Network. *Spectrochim. Acta, Part A* **2014**, *131*, 189−194.
(57) Khajeh, M.; Barkhordar, A. Modelling of Solid-Phase Tea Waste Extraction for the Removal of Manganese from Food Samples by Using Artificial Neural Network Approach. *Food Chem.* **2013**, *141*, 712−717.
(58) Sahmetlioglu, E.; Yilmaz, E.; Aktas, E.; Soylak, M. Polypyrrole/Multi-Walled Carbon Nanotube Composite for the Solid Phase Extraction of Lead(II) in Water Samples. *Talanta* **2014**, *119*, 447−451.
(59) Cavka, J. H.; Jakobsen, S.; Olsbye, U.; Guillou, N.; Lamberti, C.; Bordiga, S.; Lillerud, K. P. A New Zirconium Inorganic Building Brick Forming Metal Organic Frameworks with Exceptional Stability. *J. Am. Chem. Soc.* **2008**, *130*, 13850−13851.
(60) Arjmandi, M.; Pakizeh, M. Mixed Matrix Membranes Incorporated with Cubic-Mof-5 for Improved Polyetherimide Gas Separation Membranes: Theory and Experiment. *Ind. Eng. Chem. Res.* **2014**, *20*, 3857−3868.
(61) Naing, N. N.; Yau Li, S. F.; Lee, H. K. Magnetic Micro-Solid-Phase-Extraction of Polycyclic Aromatic Hydrocarbons in Water. *J. Chromatogr. A* **2016**, *1440*, 23−30.
(62) Poater, J.; Duran, M.; Solà, M. Aromaticity Determines the Relative Stability of Kinked Vs. Straight Topologies in Polycyclic Aromatic Hydrocarbons. *Front. Chem.* **2018**, *6*, 561.
(63) Crawford, C. B.; Quinn, B. The Interactions of Microplastics and Chemical Pollutants. In *Microplastic Pollutants*; Crawford, C. B., Quinn, B., Eds.; Elsevier: 2017; Chapter 6, pp 131−157.
(64) Pintado-Sierra, M.; Rasero-Almansa, A. M.; Corma, A.; Iglesias, M.; Sánchez, F. Bifunctional Iridium-(2-Aminoterephthalate)−Zr-Mof Chemoselective Catalyst for the Synthesis of Secondary Amines by One-Pot Three-Step Cascade Reaction. *J. Catal.* **2013**, *299*, 137−145.

https://dx.doi.org/10.1021/acsomega.0c00687
ACS Omega 2020, 5, 12202−12209